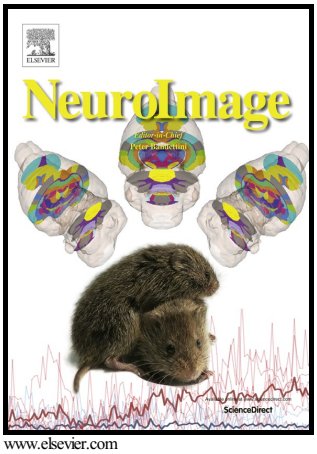

Cross-cultural consistency and diversity in Intrinsic Functional Organization of Broca's Region

Yu Zhang, Lingzhong Fan, Svenja Caspers, Stefan Heim, Ming Song, Cirong Liu, Yin Mo, Simon B. Eickhoff, Katrin Amunts, Tianzi Jiang

PII: S1053-8119(17)30153-2
DOI: http://dx.doi.org/10.1016/j.neuroimage.2017.02.042
Reference: YNIMG13827

To appear in: *NeuroImage*

Received date: 21 October 2015
Accepted date: 15 February 2017

Cite this article as: Yu Zhang, Lingzhong Fan, Svenja Caspers, Stefan Heim Ming Song, Cirong Liu, Yin Mo, Simon B. Eickhoff, Katrin Amunts and Tianz Jiang, Cross-cultural consistency and diversity in Intrinsic Functiona Organization of Broca's Region, *NeuroImage* http://dx.doi.org/10.1016/j.neuroimage.2017.02.042

Cross-cultural consistency and diversity in Intrinsic Functional Organization of Broca's Region

Yu Zhang[1,2,12], Lingzhong Fan[1], Svenja Caspers[4], Stefan Heim[4,9,10], Ming Song[1,2], Cirong Liu[7], Yin Mo[8], Simon B. Eickhoff[4,5], Katrin Amunts[4,6] and Tianzi Jiang[1,2, 3, 7, 11,*]

[1]Brainnetome Center, Institute of Automation, Chinese Academy of Sciences, Beijing 100190, China;

[2]National Laboratory of Pattern Recognition, Institute of Automation, Chinese Academy of Sciences, Beijing 100190, China;

[3]CAS Center for Excellence in Brain Science and Intelligence technology, Institute of Automation, Chinese Academy of Sciences, Beijing 100190, China;

[4]Institute of Neuroscience and Medicine (INM-1), Research Centre Juelich, 52425 Juelich, Germany;

[5]Institute for Clinical Neuroscience and Medical Psychology, Heinrich-Heine-University Düsseldorf, 40225 Düsseldorf, Germany;

[6]C. and O. Vogt Institute for Brain Research, Heinrich-Heine-University Düsseldorf, 40225 Düsseldorf, Germany;

[7]Queensland Brain Institute, The University of Queensland, QLD 4072, Australia;

[8]The First Affiliated Hospital of Kunming Medical University, Kunming 650032, China;

[9]Department of Psychiatry, Psychotherapy and Psychosomatics, Medical Faculty, RWTH Aachen, 52074 Aachen, Germany;

[10]JARA – Translational Brain Medicine, 52428 Jülich, Germany

[11]Key Laboratory for NeuroInformation of Ministry of Education, School of Life Science and Technology, University of Electronic Science and Technology of China, Chengdu 625014, China;

[12]Department of Neurology and Neurosurgery, McGill University, Montreal, Quebec H3A 2B4, Canada.

Corresponding Author: Tianzi Jiang

Brainnetome Center, National Laboratory of Pattern Recognition, Institute of Automation,

Chinese Academy of Sciences, Beijing, 100190, China

Email: jiangtz@nlpr.ia.ac.cn Telephone: +86 10 8254 4778; Fax: +86 10 8254 4777

Abstract

As a core language area, Broca's region was consistently activated in a variety of language studies even across different language systems. Moreover, a high degree of structural and functional heterogeneity in Broca's region has been reported in many studies. This raised the issue of how the intrinsic organization of Broca's region effects by different language experiences in light of its subdivisions. To address this question, we used multi-center resting-state fMRI data to explore the cross-cultural consistency and diversity of Broca's region in terms of its subdivisions, connectivity patterns and modularity organization in Chinese and German speakers. A consistent topological organization of the 13 subdivisions within the extended Broca's region was revealed on the basis of a new in-vivo parcellation map, which corresponded well to the previously reported receptorarchitectonic map. Based on this parcellation map, consistent functional connectivity patterns and modularity organization of these subdivisions were found. Some cultural difference in the functional connectivity patterns was also found, for instance stronger connectivity in Chinese subjects between area 6v2 and the motor hand area, as well as higher correlations between area 45p and middle frontal gyrus. Our study suggests that a generally invariant organization of Broca's region, together with certain regulations of different language experiences on functional connectivity, might exists to support language processing in human brain.

Keywords

Broca's region, resting-state, functional connectivity, cultural impacts, Chinese, German

Introduction

As one fundamental domain in cultural variations, language diversity has been reported in almost every linguistic aspect (Evans and Levinson, 2009; Fitch, 2011; Nettle, 1999). For instance, as a typical logographic language, Chinese maps each graphical character directly into one syllable using orthography-to-phonology transformation. Whereas, alphabetic languages like German segment each word into letters and then translate into a phonetic sequence following the grapheme-to-phoneme conversion rules (Tan et al., 2005a). Besides, Chinese has the unique characteristics of many varieties of spoken dialects assigned to the same writing systems, and using tones to distinguish between irrelevant characters. Additionally, homophones are more common in Chinese languages due to fewer distinct syllables than common written characters. The topic of how language diversity shapes the brain has attracted numerous researchers to study the underlying neural basis of language (Berwick et al., 2013; Friederici, 2011; Gomez et al., 2014; Musso et al., 2003; Nakamura et al., 2012). It has been widely reported that different language experiences were associated with various brain activations during processing of language (Paulesu et al., 2000; Tan et al., 2005a; Wu et al., 2012) and perception (Tan et al., 2008; Xue et al., 2006), diverse structural basis for dyslexia (Jednorog et al., 2015; Paulesu et al., 2001; Siok et al., 2008; Siok et al., 2004), as well as other distinct cognitive abilities (Salillas and Carreiras, 2014; Zhu et al., 2007). However, despite these cultural influences on brain mapping, a common language brain network has been revealed (Bolger et al., 2005; Paulesu et al., 2000; Tomasi and Volkow, 2012). As a core language region, Broca's region is involved in language processing across a variety of studies, for instance, during learning of new languages in both infants and adults (Dehaene-Lambertz et al., 2002; Dehaene-Lambertz et al., 2006; Gomez et al., 2014; Musso et al., 2003), and performing various language tasks across linguistic domains (Bolger et al., 2005; Price, 2012; Tan et al., 2005a). A consistent activation pattern in Broca's region has also been discovered for the processing of differential language systems, such as signed and spoken languages (Campbell et al., 2008; Neville et al., 1998; Soderfeldt et al., 1997), as well as native and second languages (Clahsen and Felser, 2006; Illes et al., 1999; Perani and Abutalebi, 2005). This study aimed to reveal the cross-cultural consistency in the intrinsic

organizational principles of Broca's region as well as the characteristics of neural plasticity in terms of different language experiences.

However, talking of "Broca's region" disregards the fact that it is a heterogeneous region in many respects. Its intrinsic architecture has been studied using histological anatomy, whereby the subdivisions were distinguished by significant changes in laminar patterns of cell bodies (cytoarchitecture) (Amunts et al., 1999; Brodmann, 1909) or in distributions of transmitter receptors (receptorarchitecture) (Amunts et al., 2010). More recently, neuroimaging studies have also revealed the non-homogeneity of Broca's region by showing different activations of its subregions in various language tasks, for instance area 44v was involved in syntax processing while the inferior frontal sulcus was associated with working memory (Clos et al., 2013; Makuuchi et al., 2009). Distinct anatomical (Anwander et al., 2007; Neubert et al., 2014) and functional connectivity profiles (Goulas et al., 2012; Klein et al., 2007) of the subdivisions in Broca's region have also been reported, for instance the engagement of area 44 in the dorsal language pathway by projecting to posterior superior temporal gyrus and the involvement of area 45 in the ventral language pathway by connecting with the anterior superior temporal gyrus. In light of the subdivisions, it is still unclear how far the fine-grained organization of Broca's region is affected by linguistic diversity.

Resting-state fMRI (rs-fMRI), which measures spontaneous fluctuations in BOLD signals, provides important insights into the core organization of the brain (van den Heuvel and Hulshoff Pol, 2010; Zhang and Raichle, 2010) and is therefore a useful tool to address the question of the cross-cultural consistency and diversity in the intrinsic organization of Broca's region. In this study, multi-center rs-fMRI data was used to test our hypothesis, including two datasets acquired in Chinese Han and Bai ethnic populations, who speak different Chinese dialects, and the other two datasets obtained from two local German groups, who are native speakers of German. We explored the cross-cultural consistency and diversity in the functional organization of Broca's region, including the topology of its subdivisions, functional connectivity patterns and modularity organization.

Materials and Methods

Data acquisition and preprocessing

Four rs-fMRI datasets from different centers were used in this study, consisting of a total of 122 healthy right-handed participants. Detailed information regarding these subjects is provided in Table 1. All subjects provided written informed consent to the study protocol as approved by the local ethics committee. The subjects were instructed to rest with their eyes closed, relax their minds, and remain as motionless as possible during the scanning. The first two datasets were acquired from two different Chinese ethnic populations using the same Philips Achieva 3.0T MRI scanner. The first dataset consisted of 29 subjects of the **Chinese Bai ethnic group** (16 males; age range = 20-36 years, mean age = 25.0, standard deviation (SD) = 4.35), who speak the **Chinese Bai language** which belongs to the Chinese-Tibetan Phylum and has its own written characters (Wang, 2004). The second dataset consisted of 29 subjects of the **Chinese Han population**, who speak **Chinese Mandarin** (14 males; age range = 22-34 years, mean age = 26.0, SD = 2.1). A total of 240 volumes, each covering the entire brain including the cerebellum with 33 axial slices, were acquired using a gradient-echo echo planar imaging (EPI) sequence [repetition time (TR) = 2.0 s, echo time (TE) = 30 ms, field of view (FOV) = 220 × 220 mm^2, matrix = 64 × 64, slice thickness = 4 mm, gap = 0.6 mm, flip angle = 90°]. A structural scan was also acquired for each participant, using a T1-weighted 3D turbo field echo (TFE) sequence (TR = 8.2 s, TE = 3.8 ms, FOV = 256 × 256 mm^2, matrix = 256 × 256, number of slices = 188, slice thickness = 1 mm, no gap, flip angle = 7°).

Using a Siemens Tim-TRIO 3.0T MRI scanner, the third dataset was acquired from 32 native speakers of German (14 males; age range = 22-39 years, mean age = 29.0, SD = 4.82), selected from a sample of 100 subjects at the Research Centre Jülich that has been used in a number of studies (Cieslik et al., 2013; Jakobs et al., 2012; Kellermann et al., 2013; Roski et al., 2013; Rottschy et al., 2013; zu Eulenburg et al., 2012). This cohort was chosen to match the age and gender of the two Chinese datasets. For each subject, 300 resting state EPI images were acquired using a gradient-echo EPI pulse sequence [TR = 2.2 s, TE = 30 ms, flip angle = 90°, in plane resolution = 3.1 × 3.1 mm^2, 36 axial slices (3.1 mm thickness) covering the entire brain]. A structural scan was also acquired for each participant, using a T1-weighted 3D

magnetization-prepared rapid acquisition with gradient echo (MPRAGE) sequence (176 axial slices, TR = 2.25 s, TE = 3.03 ms, FOV = 256 × 256 mm^2, flip angle = 9°, final voxel resolution: 1 mm × 1 mm × 1 mm).

The fourth dataset was downloaded from the 'Leipzig' dataset in the 1000 Functional Connectome Project website (www.nitrc.org/projects/fcon_1000) (Biswal et al., 2010; Kelly et al., 2012; Tomasi and Volkow, 2012). Thirty-two native speakers of German (13 males; age range = 20-31 years, mean age = 25.0, SD = 3.0), out of 37 healthy right-handed participants were selected in order to match age and gender. For each subject, 195 resting state EPI images were acquired during resting state with fixation on a cross, using a gradient-echo EPI pulse sequence [TR = 2.3 s, TE = 30 ms, flip angle = 90°, in plane resolution = 3.0 × 3.0 mm^2, 34 axial slices (4 mm thickness) covering the entire brain]. A structural scan was also acquired for each participant. More detailed description of this project and other scan parameters are available at http://www.nitrc.org/frs/?group_id=296 and http://www.nitrc.org/docman/view.php/296/719/fcon_1000_ReleaseTable_20100803.xls.

All four rs-fMRI datasets were preprocessed using the same script as described in the 1000 Functional Connectome Project (www.nitrc.org/projects/fcon_1000) (Biswal et al., 2010). The preprocessing steps included: 1) discarding the first ten volumes in each scan series for signal equilibration, 2) performing slice timing correction and motion correction, 3) removing the linear and quadratic trends, 4) band-pass temporal filtering (0.01 Hz < f < 0.08 Hz), 5) spatial smoothing using a 6-mm full-width at half-maximum (FWHM) Gaussian kernel, 6) performing nuisance signal regression [including white matter (WM), cerebrospinal fluid (CSF), the global signal, and six motion parameters], and 7) resampling into Montreal Neurological Institute (MNI) space with the concatenated transformations, including rigid transformation from the mean functional volume to the individual anatomical volume via FLIRT (Jenkinson and Smith, 2001), followed by spatial normalization of the individual anatomical volume to the MNI152 brain template (3mm isotropic resolution) using FNIRT (Andersson et al., 2007). Finally, a four-dimensional time-series dataset in standard MNI space with 3mm isotropic resolution was obtained for each subject after preprocessing.

Seed region

It has been widely accepted that two cytoarchitectonic distinct areas, i.e. area 44 and area 45 constitute the anatomy of Broca's region. In most functional studies, researchers subsume the opercular, triangular and orbital parts of the inferior frontal gyrus in the term of Broca's region (corresponding to areas 44, 45 and 47). Here, we manually delineated Broca's region and its neighboring areas according to the descriptions in the receptorarchitectonic map (Amunts et al., 2010) *following the instructions of an expert in brain anatomy*. The pial and white-matter surfaces were first reconstructed using the FreeSurfer software (https://surfer.nmr.mgh.harvard.edu/) on the basis of the MNI152 brain template with a 1mm isotropic resolution (http://www.bic.mni.mcgill.ca/ServicesAtlases/ICBM152NLin2009). The seed region was delineated on the pial surface using the following landmarks: the ventral rostral wall of the central sulcus as the posterior border, the lateral orbital sulcus as the anterior border, complete inclusion of the inferior frontal gyrus (including the opercular, triangular and orbital parts) and inferior frontal sulcus (i.e. its ventral and dorsal walls), inclusion of the frontal operculum and the transition from the frontal operculum to the anterior insula. The surface-based label file was then transformed into volume using the mri_label2vol command from Freesurfer, and extended more into the gray matter via dilation with a 3mm-sphere kernel. Additional grey-matter mask (with a threshold of 25%) was performed to exclude voxels with a high probability of white matter. The final volume was manually edited to exclude voxels within the insula by overlaying with the insular mask from the Harvard-Oxford template (Desikan et al., 2006) and then transformed into the MNI space with 3mm isotropic resolution using FLIRT (Jenkinson and Smith, 2001). Therefore, our seed region consisted of the ventral part of the precentral gyrus, the opercular, triangular and orbital parts of the inferior frontal gyrus (IFG), the inferior frontal sulcus (IFS), the inferior frontal junction (IFJ), and the frontal and central operculum (Fig. 1a).

Brain parcellation procedure using rs-fMRI data

In this study, we used a two-level parcellation scheme, including both individual- and group-level brain parcellation (Fig. 2). First, a robust parcellation procedure (Zhang et al., 2015) was applied on each subject to generate a set of individual parcellation maps. Then,

these individual parcellation results were summarized into one group parcellation map using consensus clustering (Ghaemi et al., 2009; Strehl and Ghosh, 2003).

Individual-level parcellation

In order to achieve robust brain parcellation maps for individuals, we applied the sparse representation theory to construct sparse similarity graphs on the basis of synchrony in low-frequency fluctuations of BOLD signals. Such sparse graphs could restrain noise effects on parcellation maps and also preserve inter-subject variability at the same time (Zhang et al., 2015). Then, spectral clustering was applied to these similarity graphs for clustering analysis and individual brain parcellation results were generated with predefined cluster numbers *(see below for details)*. The sensitivity and robustness of this method has been well demonstrated in our previous study (Zhang et al., 2015) on both simulated and real rs-fMRI data.

Sparse representation

The sparse representation theory (Elad, 2010) has been widely used in image processing, for instance, in classification of face, natural and medical images (Su et al., 2012; Wright et al., 2010; Wright et al., 2009), and recently been introduced into analysis of fMRI data (Li et al., 2009; Lv et al., 2015; Wee et al., 2014; Zhang et al., 2015). It employs a multivariate regression model to characterize the unique contribution of each variable in the data, different from the traditional correlation analysis conducted independently for each pair of variables regardless of the effects of other variables. In addition to this self-representation model, extra sparsity constraints on the representation coefficients as well as error terms are employed to identify the most relevant variables in the data (see Eq.1). As a result, it achieved high ability in both reducing noisy artifacts and recovering effective signals (Zhang et al., 2015). ***Importantly, both the whole-brain functional connectivity patterns and the local time-varying BOLD signals may be employed as features in our method. Here, we focus on the use of BOLD signals to illustrate the method. Specifically, the time-course of each voxel may be represented as a sparse linear combination of other voxels within the seed region (Fig. 2c), which identifies relevant voxels with similar patterns of low-frequency fluctuations in BOLD signals. The sparse representation of each voxel was calculated by solving the convex*** ℓ_1 ***-norm minimization problem (Eq.1).***

$$\min \|\mathbf{c}_i\|_1 + \|\mathbf{e}_i\|_1 \quad s.t. \quad \left\|F_{N_i}\mathbf{c}_i + \mathbf{e}_i - \mathbf{f}_i\right\|_2 \le \varepsilon \quad i = 1,...n \qquad \textbf{(Eq.1)}$$

where $\mathbf{f}_i$ ***is the feature vector of voxel*** v_i ***which could be either its time-varying BOLD signal or functional connectivity map,*** F_{N_i} ***is the dictionary matrix which includes the time-series or functional connectivity maps from all voxels within the seed region except voxel*** v_i, ε ***is a small real number to control the accuracy of the liner representation,*** $\mathbf{c}_i$ ***is the representation coefficient vector to be solved which represents the similarity between seed voxels, and*** $\mathbf{e}_i$ ***is the error term which allows noisy effects on a small number of time points or brain voxels. Additional sparsity constraints were used on both the coefficient vector*** $\|\mathbf{c}_i\|_1$ ***and the error term*** $\|e_i\|_1$.

The above objective function (Eq.1) can then be converted into an equivalent Lagrangian function:

$$\min \lambda \left\| \begin{bmatrix} \mathbf{c}_i \\ \mathbf{e}_i \end{bmatrix} \right\|_1 + \frac{1}{2} \left\| \begin{bmatrix} F_{N_i} & I \end{bmatrix} \bullet \begin{bmatrix} \mathbf{c}_i \\ \mathbf{e}_i \end{bmatrix} - \mathbf{f}_i \right\|_2^2 \quad s.t. \quad \mathbf{1}^T \mathbf{c}_i = 1, \quad i = 1,...n \qquad \textbf{(Eq.2)}$$

where the sparsity parameter λ ***is a tradeoff between the accuracy of the linear expression and the sparsity of the coefficient vector. As shown in (Zhang et al., 2015), robust parcellation was achieved on both simulated and real rs-fMRI data when the sparsity parameter was located within the interval [0.1, 1]. Here, we only showed the results by using*** $\lambda = 0.1$. ***To solve the above*** ℓ_1 ***-minimization problem (Eq.2), we used the basis pursuit denoising homotopy (BPDN-Homotopy) method (http://www.eecs.berkeley.edu/~yang/software/l1benchmark/l1benchmark.zip, (Yang et al. 2010)), which starts at the trivial solution*** $\mathbf{x}_0 = \mathbf{0}$, ***and successively builds a sparse solution by adding or removing elements from its active set until the representation error term was satisfied (Donoho and Tsaig 2008).***

The resulting coefficient vector $\mathbf{c}_i$ ***is extended into an*** n ***-dimensional vector*** $\hat{\mathbf{c}}_i$ ***by inserting a zero entry at the*** i ***-th row and further combined into a coefficient matrix***

$C = [\hat{\mathbf{c}}_1^{\,T}; \hat{\mathbf{c}}_2^{\,T}; ...; \hat{\mathbf{c}}_n^{\,T}]$ ***with zero-diagonal elements (Fig. 2c).*** Spectral clustering (Shi and Malik, 2000) was then applied to the symmetrized coefficient matrix in order to generate final parcellation results for each individual (Fig. 2d). Detailed descriptions of this method can also be found in (Zhang et al., 2015). After individual-level parcellation, the population probabilistic maps were generated by estimating the spatial distribution of each subdivision which showed the probability of how many subjects having the same labels in their individual parcellation maps.

Group-level parcellation

After the stage of individual parcellation, an additional group-level parcellation procedure was applied in order to summarize the generalized topological organization in the parcellation maps across subjects (Fig. 2e). First, the parcellation map of each individual was used to calculate a consensus matrix S , with each element $S_{ij} = 1$ if and only if voxel v_i and voxel v_j belong to the same cluster. Second, the consensus matrices from all subjects were averaged to generate a group consensus matrix, in which each element represents the percentage of two corresponding voxels belonging to the same cluster. This group consensus matrix could be treated as a group-level similarity matrix and applied to spectral clustering for the final group parcellation.

Suitable cluster number

The suitable cluster number was determined by evaluating the consistency of parcellation between randomly selected subgroups in each dataset. Specifically, a pair of parcellation maps was generated by first randomly splitting the subjects into two subgroups and then applying the above group-level parcellation procedure on each subgroup. This procedure was repeated for 100 times in order to generate a series of pairs of random subgroups and their corresponding parcellation maps. The consistency between each pair of parcellation maps was evaluated by the normalized mutual information (NMI) (Zhang et al., 2015). Two other stability indices were also tested on these parcellation results, including dice coefficient (Zhang et al., 2014) and Cramer's V (Fan et al., 2014). All three indices have values in the range [0, 1], with 0 meaning totally different parcellation patterns, and 1

meaning perfect match of the parcellation results. The mean value of the consistency indices across all random samples was calculated to represent within-group reproducibility of the parcellation map under specific cluster numbers. As considering the multi-structure organization of our seed region, we started the parcellation procedure from 6 subregions and increased the number of subdivisions until 15, which means the parcellation procedure was repeated with the cluster number assigned to each value in the range from 6 to 15. We assumed that the parcellation map with higher stability indices was more reliable. Considering the indices would decrease as the number of clusters increases, we searched for peaks instead of the highest values in the stability curve. Therefore, we identify the suitable cluster number, for each dataset separately, as the peaks in the within-group reproducibility figure.

Permutation test

The above parcellation procedure was performed on each dataset separately. In order to test the difference in parcellation maps across datasets, a permutation test was performed based on all individual parcellation results from the four datasets, under the null hypothesis that no significant difference exists among groups. A sampling distribution of the consistency values was generated by using a bootstrap-sampling procedure as follows. Two random subgroups, each consisting of 30 subjects, were sampled without replacement from the whole 122 subjects. Then, one parcellation map was generated for each subgroup by using the above group-level parcellation procedure. The consistency of parcellation between each pair of subgroups was evaluated by the stability indices. This procedure was repeated for 1000 times in order to generate a series of random samples and their corresponding consistency values. Finally, the p-value of difference in parcellation results was evaluated by calculating the percentage of permutated consistency values, out of the total number of permutations, that was smaller than the observed minimum value of consistency between datasets.

Resting-state functional connectivity

Based on the new in-vivo parcellation map of Broca's region, the functional connectivity pattern of each subdivision was analyzed on each dataset separately. To avoid possible overlapping among clusters, for each subdivision, one region of interest (ROI) was generated by first thresholding the population probabilistic map (i.e. the percentage of subjects who

showed the same labels in the individual parcellation maps) in each dataset with a probability of 50%, and then overlapping across the four datasets (as shown in Fig. S2 b). This procedure could partially rule out the mismatching of subdivisions between subjects and the effects of different brain shapes between groups after spatial registration. The mean time-course of the ROI was extracted individually to calculate the whole-brain functional connectivity using Pearson's correlation along with normalization by Fisher's z-transform. As a result, a z-score connectivity map was generated for each subdivision on each individual. Additional group analysis of these connectivity maps was performed on each dataset independently, using a one-sample t-test in SPM8 (with N = 29, 29, 32 and 32 subjects, respectively), with correction for multiple comparisons (false discovery rate (FDR) corrected p=0.01, cluster size >50 voxels by AlphaSim correction with p-value = 0.01 in the averaged brain mask with 3mm resolution). Finally, a significant functional connectivity map was generated for each subdivision on each dataset.

Statistical tests on connectivity patterns

In order to identify the common connections across different groups, a conjunction analysis using minimum statistics (Nichols et al., 2005) was performed on the connectivity maps. Specifically, for each subdivision, the t-score connectivity map from the above group analysis was first binarized (FDR corrected p=0.01, cluster size >50 voxels with the voxel-size of 3mm isotropy resolution) to represent the spatial distribution of significant connectivity patterns. Then, the binarized connectivity maps were overlapped across different datasets using the minimum statistics, e.g. between two Chinese datasets, two German datasets and among all four datasets. Only the positive functional connectivity was involved in the conjunction analysis while all anti-correlations with default mode network were neglected during analysis. Meanwhile, the contrast analysis of group differences (i.e. Chinese vs German) in functional connectivity patterns were also tested by using a two-sample t-test in SPM8 and corrected for multiple comparisons (FDR corrected p=0.01, cluster size >50 voxels). Similar conjunction and contrast analysis of functional connectivity patterns was also performed for each module within Broca's region (explained below).

Hierarchical organization

The subdivisions could be grouped into different functional modules according to spatial similarities of their functional connectivity patterns (Goulas et al., 2012; Nelson et al., 2010; Sporns, 2013). Here, we performed hierarchical clustering on the similarity matrices of connectivity patterns, and revealed a hierarchical organization among these subdivisions. Specifically, the z-score connectivity maps of each subdivision were first averaged across all subjects. Spatial similarities between these averaged connectivity maps were then assessed by using Pearson correlation and subsequent transformation into the distance measure via $1-r$, where r is the correlation coefficient. Finally, a dendrogram was constructed based on the new distance matrix by using the hierarchical clustering algorithm with "average linkage" in MATLAB (http://www.mathworks.cn/). Additional modularity analysis was performed by the modularity maximization algorithm (Newman and Girvan, 2004; Rubinov and Sporns, 2011), which automatically estimates the number of modules by optimizing the Q-function. The group averaged correlation matrices were used as the similarity measures between subdivisions. This modularity analysis was also conducted on the Chinese and German separately to assess the cross-cultural convergence and divergence in modularity organization.

Results

Consistent parcellation of Broca's region

A consistent parcellation of Broca's region was achieved on the basis of synchrony in fluctuations of time-varying BOLD signals in the four datasets acquired from different populations (Fig. 3a). The suitable number of subregions was determined by evaluating the reproducibility of parcellation among random subgroups for each dataset. Thirteen stable clusters were identified within our seed region, which showed high reproducibility on each dataset (mean NMI = 0.85, 0.83, 0.84 and 0.84, respectively, for datasets 1-4). The same conclusion was drawn by using other stability indices (Fig. S3). Besides, this parcellation map also showed high consistency across datasets (NMI = 0.89, 0.88 and 0.87, respectively, for the two Chinese datasets, two German datasets and all datasets) (Fig. 3c). Furthermore, similar parcellation map was generated by using the whole-brain functional connectivity patterns as features for clustering analysis (Fig. 4b), with a similarity of NMI = 0.82 with our current parcellation map. It is worth mentioning that, no spatial information was used in our parcellation method. These subregions were identified only by their similarities of fluctuations in time-varying BOLD signals or changes across whole-brain connectivity patterns. To confirm this, we compared our parcellation with the geometric parcellation, which constructs the similarity matrix by calculating the Euclidean-distance of the spatial coordinates between voxels and performs clustering analysis (e.g. spectral clustering) directly on the inverse of these distances (Craddock et al., 2012). The results showed a comparable pattern on the surface view (Fig. 4c), but actually a much lower similarity with our parcellation map (NMI = 0.71), which implies the mismatching of clustering between voxels in the volume space. For instance, the geometric parcellation intends to group the inferior frontal junction and frontal operculum together because of their vicinity in volume space (Fig. 4c). Meanwhile, sparse representation, using either time-varying BOLD signals or whole-brain connectivity patterns as feature, treated them as totally different functional areas. This functional separation of IFJ and op coincided with previous language studies showing that IFJ was involved in cognitive control (Brass et al., 2005; Derrfuss et al., 2005) while op was associated with grammatical processing (Friederici et al., 2006). In summary, our

parcellation maps achieved high consistency not only within each dataset (i.e. within-group reproducibility) but also between groups (i.e. between-group consistency) and even by using different features. They all differed from the geometric parcellation.

The consistency of parcellation was evaluated not only in the above group-level analysis, but also across individual parcellation maps. First of all, certain inter-individual variability of the resulting subdivisions was revealed, as shown in the population probabilistic maps (Fig. S2). For instance, large variance was found at the boundary of areas 44d and 44v, ifj1 and 45p. This variability was also present on the individual-level parcellation maps randomly selected from the four datasets (Fig. S1 d). However, no significant difference between groups was found by comparing either the principle components of individual parcellation results (Fig. S1 b) or the distributions of the similarity indices across individuals (Fig. S1 c), which both showed large overlaps across Chinese and German subjects. Moreover, the permutation test on these individual parcellation results also showed no significant difference among the four datasets (p-value = 0.563). Therefore, our parcellation map showed high consistency in both group and individual levels, but still preserved certain individual variability.

The hereby obtained parcellation map of Broca's region was compared to the parcellation scheme recently proposed based on the differential distribution of transmitter receptors (Amunts et al., 2010). We identified a very similar topological pattern with coherent spatial relations (Fig. 3b): two subregions in the ventral premotor cortex, corresponding to areas 6v1 and 6v2 of Amunts et al. 2010; two clusters at the junction of inferior frontal sulcus and precentral sulcus (IFJ), corresponding to ifj1 and ifj2; two clusters in the inferior frontal sulcus (IFS) with the caudal one covering the posterior part of IFS and corresponding to the combination of areas ifs1 and ifs2 (ifs1/2), whereas the rostral one covered the anterior part of IFS (aifs) which was still unmapped in the receptorarchitectonic map; a dorsal and ventral cluster in the opercular part of the left inferior frontal gyrus (i.e. area 44), corresponding to areas 44d and 44v; a caudal and rostral cluster in the triangular part of the left inferior frontal gyrus (i.e. area 45), corresponding to areas 45a and 45p; one cluster on the frontal operculum, corresponding to the combination of areas op8 and op9. In addition, an anterior and posterior cluster were found in the orbital part of the inferior frontal gyrus (i.e. area 47/12), which was not included in the receptorarchitectonic map (Amunts et al., 2010), but still corresponded to

architectonic subdivisions in the lateral orbital gyrus, i.e. areas 47/12a and 47/12p (Ongur et al., 2003; Petrides and Pandya, 2002). It is worth mentioning that we only achieved an approximate correspondence in spatial relations for these subdivisions. The assignment of the present clusters to the receptorarchitectonic parcellation was done by qualitative visual comparison because the 3D map of the recetorarchitecture of Broca's region is still unavailable.

Conjunction analysis on connectivity patterns

A wide range of common connections across the four datasets was identified for each subdivision by means of conjunction analysis on their functional connectivity maps (Fig. 5). In particular, area 44v showed common connections with the insular cortex, middle frontal gyrus (MFG), supramarginal gyrus (SMG), and superior temporal gyrus (STG), while area 44d showed common connections with posterior middle frontal sulcus (MFS), IFS and intraparietal sulcus (IPS). Area 45a showed common connections with the triangular and orbital parts of IFG, IFJ, posterior superior temporal sulcus (pSTS) and adjacent MTG, while area 45p showed common connections with the whole IFG, as well as IFS and IFJ. Area 47/12a showed common connections with the whole IFG, IFS and IFJ, AG, and posterior MTG, while area 47/12p showed common connections with the triangular and orbital parts of the IFG, IFJ, and posterior STS.

Cluster 6v1 showed common connections to the face area of the precentral and postcentral gyrus (Meier et al., 2008), posterior insular cortex and STG, while cluster 6v2 also showed common connections to the face area of the precentral and postcentral gyrus. Cluster ifj1 showed common connections with the orbital part of IFG, posterior IFS and MFG, and AG, while cluster ifj2 showed common connections with the triangular and orbital parts of IFG. Cluster aifs showed common connections with the opercular and triangular parts of IFG, IFS, anterior insular cortex, SMG, anterior MTG, while cluster ifs1/2 also showed common connections with the opercular and triangular parts of IFG, IFS, and IPS. Moreover, cluster op showed common connections with the opercular part of IFG and anterior insular cortex.

Contrasts on connectivity patterns

The conjunction analysis revealed a common brain network connecting with Broca's region in both Chinese and German speakers, but some culture-specific connectivity was

shown. Detailed functional connectivity maps of each subdivision for each dataset are shown in Fig. S4. In order to test the significance of differences in functional connectivity patterns between Chinese and German groups, additional two-sample t-tests were performed. Only clusters 6v2 and 45p showed significant differences in connectivity patterns between Chinese and German subjects (Fig. 6). Specifically, Chinese subjects showed significant higher connectivity with cluster 6v2 in the left precentral and postcentral gyrus, as well as the right lateral visual cortex and ITG. Stronger connectivity with cluster 45p in the left middle frontal gyrus was also detected in Chinese subjects. No significant differences were found for other subdivisions. Detailed descriptions of brain areas showing significant difference between groups can be found in Table 2. These differences were not detected intra-culturally, i.e. between either the two Chinese groups or the two German groups. Additional contrast analysis on the negative functional connectivity was also performed (Fig. S19), which was supported by studies showing an overlap between semantic network and default mode network (Wirth et al., 2011), including medial prefrontal cortex, angular gyrus and anterior temporal region.

Hierarchical organization of the subdivisions

The correlation matrices, which characterized the spatial similarities of functional connectivity maps between subdivisions, showed a similar organizational pattern across the four datasets (Fig. 7a). High consistency across language groups was shown by calculating the Pearson correlation of all connectivity values based on these correlation matrices (r=0.97 between Chinese and German datasets, only elements in the upper triangular were included in the connectivity vectors). In order to explore the hierarchical organization principles among the subdivisions, additional hierarchical clustering analysis was conducted based on the correlation matrices and a dendrogram was obtained (Fig. 7c). Similar modularity organization was also generated by using the modularity maximization algorithm (Fig. 7b), which identified five modules based on the averaged correlation matrix across the four datasets (Q=0.2540). Similar modularity was also achieved on the Chinese (Q=0.2597) and German (Q=0.2498) groups separately. A cultural-specific module consisting of area 45p was found in

Chinese groups, which was probably caused by increased functional connectivity between area 45p and MFG (Fig. 6).

A convergent hierarchical organization of the subdivisions was revealed, which consisted of five functional modules. Each module showed a distinct functional connectivity profile, but still presented high consistency across the four datasets (Fig. 8). Module 6v, consisting of clusters 6v1 and 6v2, showed significant connections with the precentral and postcentral gyrus, middle insular cortex and central operculum. Module 44v, consisting of clusters 44v and op, showed strong connections to the opercular and triangular parts of IFG, anterior IFS, anterior insular cortex, SMG and STG. Module IFS, consisting of clusters aifs, ifs1/2 and 44d, had strong connections with the whole IFG and IFS, anterior insular cortex, posterior MFS, SMG and IPS. Module IFJ, consisting of clusters ifj1 and ifj2, had significant connections with the triangular and orbital parts of IFG, IFJ, posterior MFG and AG. Module 45/47, consisting of clusters 45a/p and 47l/m, showed strong connections to the whole IFG, IFJ, posterior MFG, anterior AG, STS and posterior MTG.

The five modules also presented some cultural-specific functional connectivity (Fig. 8). To test the significance of difference in connectivity patterns, additional two-sample t-tests were performed. Only Module 6v showed significant higher connectivity in the left precentral gyrus and right anterior ITG for the Chinese subjects (FDR corrected $p=0.01$, cluster size >50 voxels) (Fig. 6 c and Table 2). These differences were neither found between the two Chinese nor the two German datasets.

Discussion

Functional parcellation of Broca's region

In the current study, we revealed a detailed parcellation of Broca's region on the basis of heterogeneity in intrinsic brain activity. Different subdivision maps of Broca's region have been proposed in the human brain, including the cytoarchitectonic (Amunts et al., 1999; Brodmann, 1909; Petrides and Pandya, 1994), receptorarchitectonic (Amunts et al., 2010) and connectivity-based parcellation (Anwander et al., 2007; Clos et al., 2013; Gorbach et al., 2011; Goulas et al., 2012; Klein et al., 2007; Neubert et al., 2014). It has been widely accepted that two cytoarchitectonically distinct areas, i.e. areas 44 and 45, constitute Broca's region. Previous connectivity-based studies also delineated the boundary between these two areas (Anwander et al., 2007; Gorbach et al., 2011; Goulas et al., 2012; Klein et al., 2007). However, the newly proposed receptorarchitectonic map revealed a considerably more detailed parcellation of an extended Broca's region, including dorsal and ventral subdivisions of area 44, and anterior and posterior subregions of area 45, as well as the subdivisions in the ventral premotor cortex, inferior frontal sulcus and frontal operculum (Amunts et al., 2010). Our study proposed a very similar parcellation map with 13 subdivisions based on rs-fMRI data (Fig. 3). Specifically, a dorsal and ventral parcellation was uncovered for the opercular part of IFG (i.e. areas 44d and 44v) and ventral premotor cortex (i.e. areas 6v1 and 6v2), and an anterior and posterior subdivision was also found for the triangular part of IFG (i.e. areas 45a and 45p) and the orbital part of IFG (i.e. areas 47/12a and 47/12p). Additional subdivisions in the inferior frontal sulcus (i.e. ifs1/2 and aifs), inferior frontal junction (i.e. ifj1 and ifj2) and frontal operculum (i.e. op) were also identified. Besides, as shown in the slice view of the parcellation map (Fig. 1D), the subdivisions of the orbital part of IFG (i.e. area 47/12) also showed a lateromedial relationship that cluster 7 (i.e. area 47/12a) located on the lateral surface of the orbital part of IFG while cluster 8 (i.e. area 47/12p) located more medially, which coincides with the idea of the lateromedial subdivision of the lateral orbital gyrus (Ongur et al., 2003). Similar anterior-posterior subdivision of area 47/12 has also been reported before (Petrides and Pandya, 2002).

Different functional specializations among these subregions have been reported in

previous task-based studies. For example, one fMRI study showed that syntactic processing was localized to area 44, while verbal working memory involved the IFS (Makuuchi et al., 2009). Another fMRI study identified a functional differentiation between area 44 and op during different types of grammatical processing (Friederici et al., 2006). Furthermore, functional subdivision of areas 6v and 44 as shown here were also supported by a meta-analytical review of functional neuroimaging language studies (Price, 2012).

In addition, we found a highly consistent topological organization of the subdivisions of Broca's region across different language groups (Figure 3a). This high consistency was present in both group- and individual-level parcellation maps. At the group level, our parcellation map was highly reproducible within each dataset and also between language groups (Figure 3c). Consistent parcellation maps were also achieved when using different features for clustering analysis, i.e. time-varying resting-state BOLD signals or whole-brain functional connectivity patterns (Figure 4). At the individual level, the parcellation maps disclosed a certain amount of inter-individual variability (Fig S2). However, the degree of variability was similar within and across language groups (Fig. S1). No significant difference between language groups has been found. Thus, this cross-cultural similarity of the present parcellation of Broca's region could provide the functional substrate for a common neural basis of language processing despite the dramatic linguistic diversity between logographic and alphabetic languages.

Connectivity profiles of Broca's region

We used our new parcellation of Broca's region to identify patterns of functional connectivity with the rest of the brain. We also found considerable overlaps across language groups in patterns of functional connectivity (Figs. 5 and 8) and modularity organization (Figs. 7 and S5). This adds support to the notion of a universal architecture of Broca's region underpinning universal language networks (Fedorenko and Thompson-Schill, 2014; Friederici, 2011; Price, 2012; Tomasi and Volkow, 2012).

The functional connectivity between Broca's region and other language areas, for instance Wernicke's area in the posterior superior temporal gyrus as well as supramarginal

gyrus and angular gyrus in the inferior parietal lobule, has been widely reported in the literature (Goulas et al., 2012; Margulies and Petrides, 2013; Tomasi and Volkow, 2012; Xiang et al., 2010). This temporal and parietal connectivity pattern of Broca's region was also revealed in our study (Fig. 5), which coincides with the dual language pathways in human and monkey tract-tracing studies (Friederici, 2011; Friederici et al., 2006; Hickok and Poeppel, 2004; Petrides and Pandya, 2009; Saur et al., 2008). For instance, the dorsal pathways project from the ventral premotor cortex (i.e. area 6v) and area 44 to the posterior STG via the arcuate fasciculus (AF) and superior longitudinal fasciculus (SLF) to support auditory-motor integration (Catani et al., 2005; Hickok and Poeppel, 2004), consistent with the overlapping functional connectivity patterns of areas 6v1 and 44v in both Chinese and German groups (Fig. 5). Moreover, the ventral pathways connect areas 45 and 47 with STG via the extreme fiber capsule system (EFCS) and uncinate fasciculus (UF) to support sound-to-meaning mapping (Hickok and Poeppel, 2004; Saur et al., 2010), coinciding with the convergent connectivity patterns of areas 45a and 47 across four groups (Fig. 5). Similar construction of these language pathways has also been reported in Chinese subjects (He et al., 2003; Qiu et al., 2011; Sun et al., 2011), which supports the cross-cultural consistency of connectivity patterns we found in Chinese and German speakers (Figs. 5 and 8).

Moreover, certain cultural-specific connectivity of Broca's region was also observed. For instance, there was stronger functional connectivity between area 6v and the motor hand area in Chinese subjects (Fig. 6), coinciding with the perspective that emphasizes the critical role of writing in Chinese language processings (Cao et al., 2013; Perfetti and Tan, 2013; Tan et al., 2005b). We also found higher connectivity between area 45p and MFG in Chinese subjects, consistent with the reports of additional brain activation of MFG during phonological processing of Chinese characters (Tan et al., 2005a; Wu et al., 2012), which additionally caused the separation of area 45p from the Module 45/47 in Chinese groups (Fig. S5). These findings of cross-cultural convergence and divergence are in line with the neuronal recycling hypothesis, according to which a core brain system of language processing exists consisting of intrinsic anatomical and connectional constraints, but different experiences of culture and training would regulate its neural plasticity by recycling of the existing neural substrates (Dehaene and Cohen, 2007; Dehaene et al., 2010).

Modularity organization of Broca's region

In addition to the functional connectivity analysis, we also performed hierarchical organization analysis to identify the modular architecture of Broca's region. Five functional modules were identified within Broca's region, which followed a consistent pattern across the different language groups (Fig. S5). We then identified the functional connectivity pattern of each module with the rest of the brain. Each module had a different connectivity profile (Fig. 8) possibly supporting their characterized functions involved in different aspects of language processing. Specifically, Module 6v had strong connections with the precentral and postcentral gyrus, and most likely participates in motor execution and planning during word articulation (Hickok et al., 2011; Price, 2012; Scott et al., 2009). Module 44v was highly connected to SMG and STG, and is thought to be involved in the syntax processing (Fiebach et al., 2004; Makuuchi et al., 2009) and syllabic verbal utterances (Moser et al., 2009; Riecker et al., 2008). Module IFS had strong connections with posterior MFS, SMG and IPS, and is possibly associated with verbal working memory (Makuuchi et al., 2009; Paulesu et al., 1993) and linguistic sequencing (syllabification) (Callan et al., 2006; Indefrey and Levelt, 2004). Module IFJ had significant connections with the posterior MFG, AG and posterior MTG, and is known to be activated in cognitive control including task switching and shifting (Brass et al., 2005; Derrfuss et al., 2005) and attention (Heim et al., 2014). Module 45/47 was strongly connected to posterior MFG, AG, STS and posterior MTG, and is typically associated with semantic processing (Bookheimer, 2002; Dapretto and Bookheimer, 1999; Price, 2012). However, a cultural-specific module was found in Chinese groups, i.e. area 45p was separated from the original module 45/47 (Fig. S5). This variation in modularity is probably caused by the higher functional connectivity between area 45p and MFG in Chinese subjects (Fig. 6). Future research will be necessary to detect its specific role in Chinese language processing.

Moreover, this fine-grained modularity analysis concurs with the theory of a functional specialization language networks into language-specific and domain-general subnetworks (Fedorenko and Thompson-Schill, 2014). Among the present five modules, three correspond to domain-general modules, including Modules 6v, IFS and IFJ, which generally support motor execution, working memory and cognitive control (Fedorenko and Thompson-Schill,

2014), whereas the other two modules, i.e. Module 44v and Module 45/47, are associated with specific aspects of language processing such as syntactic and semantic processing (Fedorenko et al., 2012). A similar hierarchical organization pattern within Broca's region has also been proposed by Amunts (Amunts et al., 2010; Amunts and Zilles, 2012) based on the distribution of neurotransmitter receptors. Thus, this coherent modularity organization of Broca's region could provide new insights into its universal behaviors in language processing.

In conclusion, the present study revealed a common intrinsic organization of Broca's region across logographic and alphabetic languages, including similar topology of the parcellation maps, consistent connectivity patterns of the subdivisions and convergent modularity organization. Our study provides a neuroanatomical insight into the consistent involvement of Broca's region across different languages and may thus contribute to the understanding of the neural basis of language universals. Future research will be necessary in order to determine whether other language areas beyond Broca's region also share a common pattern of organization. The same line of reasoning applies for studies involving other languages, which are necessary in order to solve the debate on the universal brain basis for all language processing (Nakamura et al., 2012; Perfetti and Tan, 2013).

Limitations

In this study, although all subjects were scanned at 3.0T and using the EPI sequence, the four rs-fMRI datasets were not collected from the same center or using the same scanner or using the same protocols. This might cause bias in functional connectivity analysis due to different scanning conditions and variations in SNR of fMRI signals. However, no systemic bias was found during the analysis. Instead, we found highly consistent parcellation maps across the four groups, as well as large overlaps in the connectivity patterns of the subdivisions and modules. Moreover, the difference in the connectivity profiles was region-specific, e.g. only present in the dorsal subdivision of area 6v and the posterior subdivision of area 45. One might expect more general scanner-specific effects which could affect all connectivity measures. Instead, only two out of thirteen subregions showed a group

difference in connectivity patterns. Thus, this cross-cultural consistency and diversity analysis of Broca's region could still be valid despite possible differences in scanning conditions across multiple datasets. However, considering the limitations of using multi-site resting-state fMRI in studying language pathways and functions, our results on cross-cultural differences still need to be interpreted with caution.

Acknowledgments

We thank Dr. Alain Dagher for his helpful comments during the revision of the manuscript. This work was supported by the Natural Science Foundation of China (91432302, 31620103905), the Strategic Priority Research Program of the Chinese Academy of Sciences (Grant No. XDB02030300), Key Research Program of Frontier Sciences of the Chinese Academy of Sciences（Grant No. QYZDJ-SSW-SMC019）and Beijing Municipal Science & Technology Commission (Grant No. Z161100000216139).

The authors declare no competing financial interests.

References

Amunts, K., Lenzen, M., Friederici, A.D., Schleicher, A., Morosan, P., Palomero-Gallagher, N., Zilles, K., 2010. Broca's region: novel organizational principles and multiple receptor mapping. PLoS Biol 8,e1000489.

Amunts, K., Schleicher, A., Burgel, U., Mohlberg, H., Uylings, H.B., Zilles, K., 1999. Broca's region revisited: cytoarchitecture and intersubject variability. J Comp Neurol 412, 319-341.

Amunts, K., Zilles, K., 2012. Architecture and organizational principles of Broca's region. Trends in Cognitive Sciences 16, 418-426.

Andersson, J.L., Jenkinson, M., Smith, S., 2007. Non-linear registration, aka Spatial normalisation FMRIB technical report TR07JA2. FMRIB Analysis Group of the University of Oxford.

Anwander, A., Tittgemeyer, M., von Cramon, D.Y., Friederici, A.D., Knosche, T.R., 2007. Connectivity-Based Parcellation of Broca's Area. Cereb Cortex 17, 816-825.

Berwick, R.C., Friederici, A.D., Chomsky, N., Bolhuis, J.J., 2013. Evolution, brain, and the nature of language. Trends in Cognitive Sciences 17, 89-98.

Biswal, B.B., Mennes, M., Zuo, X.N., Gohel, S., Kelly, C., Smith, S.M., Beckmann, C.F., Adelstein, J.S., Buckner, R.L., Colcombe, S., Dogonowski, A.M., Ernst, M., Fair, D., Hampson, M., Hoptman, M.J., Hyde, J.S., Kiviniemi, V.J., Kotter, R., Li, S.J., Lin, C.P., Lowe, M.J., Mackay, C., Madden, D.J., Madsen, K.H., Margulies, D.S., Mayberg, H.S., McMahon, K., Monk, C.S., Mostofsky, S.H., Nagel, B.J., Pekar, J.J., Peltier, S.J., Petersen, S.E., Riedl, V., Rombouts, S.A., Rypma, B., Schlaggar, B.L., Schmidt, S., Seidler, R.D., Siegle, G.J., Sorg, C., Teng, G.J., Veijola, J., Villringer, A., Walter, M., Wang, L., Weng, X.C., Whitfield-Gabrieli, S., Williamson, P., Windischberger, C., Zang, Y.F., Zhang, H.Y., Castellanos, F.X., Milham, M.P., 2010. Toward discovery science of human brain function. Proc Natl Acad Sci U S A 107, 4734-4739.

Bolger, D.J., Perfetti, C.A., Schneider, W., 2005. Cross-cultural effect on the brain revisited: universal structures plus writing system variation. Hum Brain Mapp 25, 92-104.

Bookheimer, S., 2002. Functional MRI of language: new approaches to understanding the cortical organization of semantic processing. Annu Rev Neurosci 25, 151-188.

Brass, M., Derrfuss, J., Forstmann, B., von Cramon, D.Y., 2005. The role of the inferior frontal junction area in cognitive control. Trends in Cognitive Sciences 9, 314-316.

Brodmann, K., 1909. Vergleichende Lokalisationslehre der Großhirnrinde in ihren Prinzipien dargestellt auf Grund des Zellenbaues. Barth, Leipzig (Germany).

Callan, D.E., Tsytsarev, V., Hanakawa, T., Callan, A.M., Katsuhara, M., Fukuyama, H., Turner, R., 2006. Song and speech: brain regions involved with perception and covert production. Neuroimage 31, 1327-1342.

Campbell, R., MacSweeney, M., Waters, D., 2008. Sign language and the brain: a review. J

Deaf Stud Deaf Educ 13, 3-20.

Cao, F., Vu, M., Chan, D.H., Lawrence, J.M., Harris, L.N., Guan, Q., Xu, Y., Perfetti, C.A., 2013. Writing affects the brain network of reading in Chinese: a functional magnetic resonance imaging study. Hum Brain Mapp 34, 1670-1684.

Catani, M., Jones, D.K., ffytche, D.H., 2005. Perisylvian language networks of the human brain. Ann Neurol 57, 8-16.

Cieslik, E.C., Zilles, K., Caspers, S., Roski, C., Kellermann, T.S., Jakobs, O., Langner, R., Laird, A.R., Fox, P.T., Eickhoff, S.B., 2013. Is there "one" DLPFC in cognitive action control? Evidence for heterogeneity from co-activation-based parcellation. Cereb Cortex 23, 2677-2689.

Clahsen, H., Felser, C., 2006. How native-like is non-native language processing? Trends in Cognitive Sciences 10, 564-570.

Clos, M., Amunts, K., Laird, A.R., Fox, P.T., Eickhoff, S.B., 2013. Tackling the multifunctional nature of Broca's region meta-analytically: co-activation-based parcellation of area 44. Neuroimage 83, 174-188.

Craddock, R.C., James, G.A., Holtzheimer, P.E., 3rd, Hu, X.P., Mayberg, H.S., 2012. A whole brain fMRI atlas generated via spatially constrained spectral clustering. Hum Brain Mapp 33, 1914-1928.

Dapretto, M., Bookheimer, S.Y., 1999. Form and content: dissociating syntax and semantics in sentence comprehension. Neuron 24, 427-432.

Dehaene-Lambertz, G., Dehaene, S., Hertz-Pannier, L., 2002. Functional neuroimaging of speech perception in infants. Science 298, 2013-2015.

Dehaene-Lambertz, G., Hertz-Pannier, L., Dubois, J., Meriaux, S., Roche, A., Sigman, M., Dehaene, S., 2006. Functional organization of perisylvian activation during presentation of sentences in preverbal infants. Proc Natl Acad Sci U S A 103, 14240-14245.

Dehaene, S., Cohen, L., 2007. Cultural recycling of cortical maps. Neuron 56, 384-398.

Dehaene, S., Pegado, F., Braga, L.W., Ventura, P., Nunes Filho, G., Jobert, A., Dehaene-Lambertz, G., Kolinsky, R., Morais, J., Cohen, L., 2010. How learning to read changes the cortical networks for vision and language. Science 330, 1359-1364.

Derrfuss, J., Brass, M., Neumann, J., von Cramon, D.Y., 2005. Involvement of the inferior frontal junction in cognitive control: meta-analyses of switching and Stroop studies. Hum Brain Mapp 25, 22-34.

Desikan, R.S., Segonne, F., Fischl, B., Quinn, B.T., Dickerson, B.C., Blacker, D., Buckner, R.L., Dale, A.M., Maguire, R.P., Hyman, B.T., Albert, M.S., Killiany, R.J., 2006. An automated labeling system for subdividing the human cerebral cortex on MRI scans into gyral based regions of interest. Neuroimage 31, 968-980.

Elad, M., 2010. Sparse and redundant representations: from theory to applications in signal and

image processing. Springer.

Evans, N., Levinson, S.C., 2009. The myth of language universals: language diversity and its importance for cognitive science. Behavioral and Brain Sciences 32, 429-448; discussion 448-494.

Fan, L., Wang, J., Zhang, Y., Han, W., Yu, C., Jiang, T., 2014. Connectivity-based parcellation of the human temporal pole using diffusion tensor imaging. Cereb Cortex 24, 3365-3378.

Fedorenko, E., Duncan, J., Kanwisher, N., 2012. Language-selective and domain-general regions lie side by side within Broca's area. Curr Biol 22, 2059-2062.

Fedorenko, E., Thompson-Schill, S.L., 2014. Reworking the language network. Trends in Cognitive Sciences 18, 120-126.

Fiebach, C.J., Vos, S.H., Friederici, A.D., 2004. Neural correlates of syntactic ambiguity in sentence comprehension for low and high span readers. J Cogn Neurosci 16, 1562-1575.

Fitch, W.T., 2011. Unity and diversity in human language. Philos Trans R Soc Lond B Biol Sci 366, 376-388.

Friederici, A.D., 2011. The brain basis of language processing: from structure to function. Physiological Reviews 91, 1357-1392.

Friederici, A.D., Bahlmann, J., Heim, S., Schubotz, R.I., Anwander, A., 2006. The brain differentiates human and non-human grammars: functional localization and structural connectivity. Proc Natl Acad Sci U S A 103, 2458-2463.

Ghaemi, R., Sulaiman, M.N., Ibrahim, H., Mustapha, N., 2009. A survey: clustering ensembles techniques. World Academy of Science, Engineering and Technology 50, 636-645.

Gomez, D.M., Berent, I., Benavides-Varela, S., Bion, R.A., Cattarossi, L., Nespor, M., Mehler, J., 2014. Language universals at birth. Proc Natl Acad Sci U S A 111, 5837-5841.

Gorbach, N.S., Schutte, C., Melzer, C., Goldau, M., Sujazow, O., Jitsev, J., Douglas, T., Tittgemeyer, M., 2011. Hierarchical information-based clustering for connectivity-based cortex parcellation. Front Neuroinform 5, 18.

Goulas, A., Uylings, H.B., Stiers, P., 2012. Unravelling the intrinsic functional organization of the human lateral frontal cortex: a parcellation scheme based on resting state FMRI. J Neurosci 32, 10238-10252.

He, A.G., Tan, L.H., Tang, Y., James, G.A., Wright, P., Eckert, M.A., Fox, P.T., Liu, Y., 2003. Modulation of neural connectivity during tongue movement and reading. Hum Brain Mapp 18, 222-232.

Heim, S., Pape-Neumann, J., van Ermingen-Marbach, M., Brinkhaus, M., Grande, M., 2014. Shared vs. specific brain activation changes in dyslexia after training of phonology, attention, or reading. Brain Struct Funct.

Hickok, G., Houde, J., Rong, F., 2011. Sensorimotor integration in speech processing: computational basis and neural organization. Neuron 69, 407-422.

Hickok, G., Poeppel, D., 2004. Dorsal and ventral streams: a framework for understanding aspects of the functional anatomy of language. Cognition 92, 67-99.

Illes, J., Francis, W.S., Desmond, J.E., Gabrieli, J.D., Glover, G.H., Poldrack, R., Lee, C.J., Wagner, A.D., 1999. Convergent cortical representation of semantic processing in bilinguals. Brain Lang 70, 347-363.

Indefrey, P., Levelt, W.J., 2004. The spatial and temporal signatures of word production components. Cognition 92, 101-144.

Jakobs, O., Langner, R., Caspers, S., Roski, C., Cieslik, E.C., Zilles, K., Laird, A.R., Fox, P.T., Eickhoff, S.B., 2012. Across-study and within-subject functional connectivity of a right temporo-parietal junction subregion involved in stimulus-context integration. Neuroimage 60, 2389-2398.

Jednorog, K., Marchewka, A., Altarelli, I., Monzalvo Lopez, A.K., van Ermingen-Marbach, M., Grande, M., Grabowska, A., Heim, S., Ramus, F., 2015. How reliable are gray matter disruptions in specific reading disability across multiple countries and languages? Insights from a large-scale voxel-based morphometry study. Hum Brain Mapp 36, 1741-1754.

Jenkinson, M., Smith, S., 2001. A global optimisation method for robust affine registration of brain images. Med Image Anal 5, 143-156.

Kellermann, T.S., Caspers, S., Fox, P.T., Zilles, K., Roski, C., Laird, A.R., Turetsky, B.I., Eickhoff, S.B., 2013. Task- and resting-state functional connectivity of brain regions related to affection and susceptible to concurrent cognitive demand. Neuroimage 72, 69-82.

Kelly, C., Toro, R., Di Martino, A., Cox, C.L., Bellec, P., Castellanos, F.X., Milham, M.P., 2012. A convergent functional architecture of the insula emerges across imaging modalities. Neuroimage 61, 1129-1142.

Klein, J.C., Behrens, T.E., Robson, M.D., Mackay, C.E., Higham, D.J., Johansen-Berg, H., 2007. Connectivity-based parcellation of human cortex using diffusion MRI: Establishing reproducibility, validity and observer independence in BA 44/45 and SMA/pre-SMA. Neuroimage 34, 204-211.

Li, Y., Namburi, P., Yu, Z., Guan, C., Feng, J., Gu, Z., 2009. Voxel selection in FMRI data analysis based on sparse representation. IEEE Trans Biomed Eng 56, 2439-2451.

Lv, J., Jiang, X., Li, X., Zhu, D., Chen, H., Zhang, T., Zhang, S., Hu, X., Han, J., Huang, H., Zhang, J., Guo, L., Liu, T., 2015. Sparse representation of whole-brain fMRI signals for identification of functional networks. Med Image Anal 20, 112-134.

Makuuchi, M., Bahlmann, J., Anwander, A., Friederici, A.D., 2009. Segregating the core computational faculty of human language from working memory. Proc Natl Acad Sci U S A 106, 8362-8367.

Margulies, D.S., Petrides, M., 2013. Distinct parietal and temporal connectivity profiles of ventrolateral frontal areas involved in language production. J Neurosci 33, 16846-16852.

Meier, J.D., Aflalo, T.N., Kastner, S., Graziano, M.S., 2008. Complex organization of human

primary motor cortex: a high-resolution fMRI study. J Neurophysiol 100, 1800-1812.

Moser, D., Baker, J.M., Sanchez, C.E., Rorden, C., Fridriksson, J., 2009. Temporal order processing of syllables in the left parietal lobe. J Neurosci 29, 12568-12573.

Musso, M., Moro, A., Glauche, V., Rijntjes, M., Reichenbach, J., Buchel, C., Weiller, C., 2003. Broca's area and the language instinct. Nat Neurosci 6, 774-781.

Nakamura, K., Kuo, W.J., Pegado, F., Cohen, L., Tzeng, O.J., Dehaene, S., 2012. Universal brain systems for recognizing word shapes and handwriting gestures during reading. Proc Natl Acad Sci U S A 109, 20762-20767.

Nelson, S.M., Cohen, A.L., Power, J.D., Wig, G.S., Miezin, F.M., Wheeler, M.E., Velanova, K., Donaldson, D.I., Phillips, J.S., Schlaggar, B.L., Petersen, S.E., 2010. A parcellation scheme for human left lateral parietal cortex. Neuron 67, 156-170.

Nettle, D., 1999. Linguistic diversity. Oxford University Press, Oxford ; New York.

Neubert, F.X., Mars, R.B., Thomas, A.G., Sallet, J., Rushworth, M.F., 2014. Comparison of human ventral frontal cortex areas for cognitive control and language with areas in monkey frontal cortex. Neuron 81, 700-713.

Neville, H.J., Bavelier, D., Corina, D., Rauschecker, J., Karni, A., Lalwani, A., Braun, A., Clark, V., Jezzard, P., Turner, R., 1998. Cerebral organization for language in deaf and hearing subjects: biological constraints and effects of experience. Proc Natl Acad Sci U S A 95, 922-929.

Nichols, T., Brett, M., Andersson, J., Wager, T., Poline, J.B., 2005. Valid conjunction inference with the minimum statistic. Neuroimage 25, 653-660.

Ongur, D., Ferry, A.T., Price, J.L., 2003. Architectonic subdivision of the human orbital and medial prefrontal cortex. J Comp Neurol 460, 425-449.

Paulesu, E., Demonet, J.F., Fazio, F., McCrory, E., Chanoine, V., Brunswick, N., Cappa, S.F., Cossu, G., Habib, M., Frith, C.D., Frith, U., 2001. Dyslexia: cultural diversity and biological unity. Science 291, 2165-2167.

Paulesu, E., Frith, C.D., Frackowiak, R.S., 1993. The neural correlates of the verbal component of working memory. Nature 362, 342-345.

Paulesu, E., McCrory, E., Fazio, F., Menoncello, L., Brunswick, N., Cappa, S.F., Cotelli, M., Cossu, G., Corte, F., Lorusso, M., Pesenti, S., Gallagher, A., Perani, D., Price, C., Frith, C.D., Frith, U., 2000. A cultural effect on brain function. Nat Neurosci 3, 91-96.

Perani, D., Abutalebi, J., 2005. The neural basis of first and second language processing. Curr Opin Neurobiol 15, 202-206.

Perfetti, C.A., Tan, L.H., 2013. Write to read: the brain's universal reading and writing network. Trends in Cognitive Sciences 17, 56-57.

Petrides, M., Pandya, D.N., 1994. Comparative architectonic analysis of the human and the macaque frontal cortex. In: Boller F, J, G. (Eds.), Handbook of neuropsychology. Elsevier,

Amsterdam, pp. 17-58.

Petrides, M., Pandya, D.N., 2002. Comparative cytoarchitectonic analysis of the human and the macaque ventrolateral prefrontal cortex and corticocortical connection patterns in the monkey. Eur J Neurosci 16, 291-310.

Petrides, M., Pandya, D.N., 2009. Distinct parietal and temporal pathways to the homologues of Broca's area in the monkey. PLoS Biol 7, e1000170.

Price, C.J., 2012. A review and synthesis of the first 20 years of PET and fMRI studies of heard speech, spoken language and reading. Neuroimage 62, 816-847.

Qiu, D., Tan, L.H., Siok, W.T., Zhou, K., Khong, P.L., 2011. Lateralization of the arcuate fasciculus and its differential correlation with reading ability between young learners and experienced readers: a diffusion tensor tractography study in a Chinese cohort. Hum Brain Mapp 32, 2054-2063.

Riecker, A., Brendel, B., Ziegler, W., Erb, M., Ackermann, H., 2008. The influence of syllable onset complexity and syllable frequency on speech motor control. Brain Lang 107, 102-113.

Roski, C., Caspers, S., Langner, R., Laird, A.R., Fox, P.T., Zilles, K., Amunts, K., Eickhoff, S.B., 2013. Adult age-dependent differences in resting-state connectivity within and between visual-attention and sensorimotor networks. Front Aging Neurosci 5, 67.

Rottschy, C., Caspers, S., Roski, C., Reetz, K., Dogan, I., Schulz, J.B., Zilles, K., Laird, A.R., Fox, P.T., Eickhoff, S.B., 2013. Differentiated parietal connectivity of frontal regions for "what" and "where" memory. Brain Struct Funct 218, 1551-1567.

Salillas, E., Carreiras, M., 2014. Core number representations are shaped by language. Cortex 52, 1-11.

Saur, D., Kreher, B.W., Schnell, S., Kummerer, D., Kellmeyer, P., Vry, M.S., Umarova, R., Musso, M., Glauche, V., Abel, S., Huber, W., Rijntjes, M., Hennig, J., Weiller, C., 2008. Ventral and dorsal pathways for language. Proc Natl Acad Sci U S A 105, 18035-18040.

Saur, D., Schelter, B., Schnell, S., Kratochvil, D., Kupper, H., Kellmeyer, P., Kummerer, D., Kloppel, S., Glauche, V., Lange, R., Mader, W., Feess, D., Timmer, J., Weiller, C., 2010. Combining functional and anatomical connectivity reveals brain networks for auditory language comprehension. Neuroimage 49, 3187-3197.

Scott, S.K., McGettigan, C., Eisner, F., 2009. A little more conversation, a little less action--candidate roles for the motor cortex in speech perception. Nat Rev Neurosci 10, 295-302.

Shi, J.B., Malik, J., 2000. Normalized cuts and image segmentation. Ieee Transactions on Pattern Analysis and Machine Intelligence 22, 888-905.

Siok, W.T., Niu, Z., Jin, Z., Perfetti, C.A., Tan, L.H., 2008. A structural-functional basis for dyslexia in the cortex of Chinese readers. Proc Natl Acad Sci U S A 105, 5561-5566.

Siok, W.T., Perfetti, C.A., Jin, Z., Tan, L.H., 2004. Biological abnormality of impaired reading

is constrained by culture. Nature 431, 71-76.

Soderfeldt, B., Ingvar, M., Ronnberg, J., Eriksson, L., Serrander, M., Stone-Elander, S., 1997. Signed and spoken language perception studied by positron emission tomography. Neurology 49, 82-87.

Sporns, O., 2013. Network attributes for segregation and integration in the human brain. Curr Opin Neurobiol 23, 162-171.

Strehl, A., Ghosh, J., 2003. Cluster ensembles --- a knowledge reuse framework for combining multiple partitions. J. Mach. Learn. Res. 3, 583-617.

Su, L., Wang, L., Chen, F., Shen, H., Li, B., Hu, D., 2012. Sparse representation of brain aging: extracting covariance patterns from structural MRI. PLoS One 7, e36147.

Sun, Y., Yang, Y., Desroches, A.S., Liu, L., Peng, D., 2011. The role of the ventral and dorsal pathways in reading Chinese characters and English words. Brain Lang 119, 80-88.

Tan, L.H., Chan, A.H., Kay, P., Khong, P.L., Yip, L.K., Luke, K.K., 2008. Language affects patterns of brain activation associated with perceptual decision. Proc Natl Acad Sci U S A 105, 4004-4009.

Tan, L.H., Laird, A.R., Li, K., Fox, P.T., 2005a. Neuroanatomical correlates of phonological processing of Chinese characters and alphabetic words: a meta-analysis. Hum Brain Mapp 25, 83-91.

Tan, L.H., Spinks, J.A., Eden, G.F., Perfetti, C.A., Siok, W.T., 2005b. Reading depends on writing, in Chinese. Proc Natl Acad Sci U S A 102, 8781-8785.

Tomasi, D., Volkow, N.D., 2012. Resting functional connectivity of language networks: characterization and reproducibility. Mol Psychiatry 17, 841-854.

van den Heuvel, M.P., Hulshoff Pol, H.E., 2010. Exploring the brain network: a review on resting-state fMRI functional connectivity. Eur Neuropsychopharmacol 20, 519-534.

Wang, F., 2004. Language Policy for Bai. Language Policy in the People's Republic of China. Springer, pp. 277-287.

Wee, C.Y., Yap, P.T., Zhang, D., Wang, L., Shen, D., 2014. Group-constrained sparse fMRI connectivity modeling for mild cognitive impairment identification. Brain Struct Funct 219, 641-656.

Wirth, M., Jann, K., Dierks, T., Federspiel, A., Wiest, R., Horn, H., 2011. Semantic memory involvement in the default mode network: a functional neuroimaging study using independent component analysis. Neuroimage 54, 3057-3066.

Wright, J., Ma, Y., Mairal, J., Sapiro, G., Huang, T.S., Yan, S., 2010. Sparse representation for computer vision and pattern recognition. Proceedings of the IEEE, pp. 1031-1044.

Wright, J., Yang, A.Y., Ganesh, A., Sastry, S.S., Ma, Y., 2009. Robust Face Recognition via Sparse Representation. IEEE Trans Pattern Anal Mach Intell 31, 210-227.

Wu, C.Y., Ho, M.H., Chen, S.H., 2012. A meta-analysis of fMRI studies on Chinese orthographic, phonological, and semantic processing. Neuroimage 63, 381-391.

Xiang, H.D., Fonteijn, H.M., Norris, D.G., Hagoort, P., 2010. Topographical functional connectivity pattern in the perisylvian language networks. Cereb Cortex 20, 549-560.

Xue, G., Chen, C., Jin, Z., Dong, Q., 2006. Language experience shapes fusiform activation when processing a logographic artificial language: an fMRI training study. Neuroimage 31, 1315-1326.

Zhang, D., Raichle, M.E., 2010. Disease and the brain's dark energy. Nat Rev Neurol 6, 15-28.

Zhang, Y., Caspers, S., Fan, L.Z., Fan, Y., Song, M., Liu, C.R., Mo, Y., Roski, C., Eickhoff, S., Amunts, K., Jiang, T.Z., 2015. Robust brain parcellation using sparse representation on resting-state fMRI. Brain Struct Funct 220, 3565-3579.

Zhang, Y., Fan, L., Zhang, Y., Wang, J., Zhu, M., Zhang, Y., Yu, C., Jiang, T., 2014. Connectivity-based parcellation of the human posteromedial cortex. Cereb Cortex 24, 719-727.

Zhu, Y., Zhang, L., Fan, J., Han, S., 2007. Neural basis of cultural influence on self-representation. Neuroimage 34, 1310-1316.

zu Eulenburg, P., Caspers, S., Roski, C., Eickhoff, S.B., 2012. Meta-analytical definition and functional connectivity of the human vestibular cortex. Neuroimage 60, 162-169.

Figure Legends

Figure 1. Definition and parcellation of Broca's region.

Our seed region included the ventral part of the precentral gyrus, the opercular, triangular and orbital parts of the inferior frontal gyrus, the inferior frontal sulcus and junction areas, and the frontal and central operculum. The seed region was manually delineated on the basis of the averaged T1 images of MNI152 brain template and edited to exclude voxels from the insula. The seed region was shown on the lateral surface view (A) as well as the coronal and axial slice views (B) which were both overlapped on the averaged MNI152 brain. The consistent parcellation map of Broca's region across the four rs-fMRI datasets was also shown on lateral surface view (C) as well as the coronal and axial slice views (D).

Figure 2. Parcellation scheme when using sparse representation on rs-fMRI data.

The procedure includes a two-level brain parcellation scheme. The first row presents the process for individual parcellation. Specifically, after defining the seed region (A), we extracted the BOLD signal of each voxel within the seed region (B) and calculated its representation coefficients by searching across the entire seed region based on the sparse representation theory (C). A sparse similarity matrix was constructed based on these representation coefficients and spectral clustering was applied to generate individual parcellation for each subject (D). The second row shows the procedure of group-level parcellation in order to summarize the generalized topology of subdivisions across subjects. Specifically, a consensus matrix was calculated from the individual parcellation map of each subject and averaged across all subjects in the whole group (E). This averaged consensus matrix was then applied to spectral clustering for the group parcellation map (F). See ***Materials and Methods*** for more detailed explanations of this parcellation method.

Figure 3. Consistent parcellation of Broca's region on the four rs-fMRI datasets acquired from Chinese and German populations.

(A) Group parcellation map of Broca's region on each of the four rs-fMRI datasets which should high consistency between language groups. (B) The convergent parcellation map of Broca's region among these four datasets, which consisted of 13 subdivisions, including dorsal and ventral area 44, anterior and posterior area 45, anterior and posterior area 47/12, and two subregions within area 6v, four clusters within IFS and IFJ, as well as a cluster in the frontal and central operculum. This in-vivo parcellation map achieved high correspondence to the receptorarchitectonic map (adapted from (Amunts et al., 2010) with permission from the author). (C) The reproducibility of parcellation results was calculated separately for each dataset, which indicated k =13 was the suitable cluster number. High consistency of these parcellation maps was also archived within and between language groups.

Figure 4. Comparison of parcellation maps generated by using different features.

Similar parcellation maps were generated by using local time-varying resting-state BOLD signals (A) or whole-brain functional connectivity patterns (B). A high similarity of NMI = 0.82 was archived between these two maps. In the meanwhile, the geometric parcellation of Broca's region was also present (C), which constructs the similarity matrix by calculating the Euclidean-distance of the spatial coordinates between voxels and performs clustering analysis directly on the distance matrix. A much lower similarity between the geometric parcellation with our current parcellation map was archived (NMI = 0.71). A detailed comparison of these parcellation maps was also shown in the slice view (D). As marked in the red circle, the geometric parcellation intends to group the inferior frontal junction and frontal operculum together because of their vicinity in volume space. Meanwhile, sparse representation, using either time-varying BOLD signals or whole-brain connectivity patterns as feature, treated them as totally different functional areas. CBP-fMRI, brain parcellation using local time-varying resting-state BOLD signals as features; CBP-RSFC, brain parcellation using whole-brain functional connectivity patterns as features; CBP-Spatial, brain parcellation only using spatial coordinates of the seed voxels as features.

Figure 5. Conjunction analysis of functional connectivity patterns for each subdivision.

Common connections for each of the thirteen subdivisions was present for the Chinese datasets (green), German datasets (blue) and across all four datasets (red). For each pair of figures, the first column shows the location of the subdivision on the lateral surface view, and the second column shows the conjunction analysis of its significant functional connectivity patterns across the four datasets which was binarized first with multiple comparison corrections (FDR p=0.01, cluster size >50 with 3mm isotropic resolution).

Figure 6. Significant differences in functional connectivity profiles between Chinese and German groups.

Two-sample t-tests were performed for each subdivision and each module within Broca's region to test the significance of differences in the functional connectivity patterns between Chinese and German groups. Only clusters 6v2 and 45p and Module 6v showed significant differences between Chinese and German subjects after multiple comparison corrections (FDR p=0.01, cluster size >50 with 3mm isotropic resolution). Specifically, in Chinese subjects, cluster 6v2 showed higher connectivity with the left precentral and postcentral gyrus, as well as the right lateral visual cortex and inferior temporal gyrus. Cluster 45p showed stronger functional connectivity with the left middle frontal gyrus in Chinese subjects. Module 6v showed significant higher connectivity with the left precentral gyrus and right inferior temporal gyrus in the Chinese subjects. The explicit spatial coordinates of these regions of difference in functional connectivity can be found in Table 2.

Figure 7. Hierarchical organization of the subdivisions within Broca's region.

(A) Correlation matrices presenting the spatial similarity of the functional connectivity patterns between each pair of the thirteen subdivisions on the four datasets. (B) Modularity analysis of the subdivisions within Broca's region. (C) Hierarchical organization pattern among these subdivisions. Five functional modules were identified within Broca's region based on the averaged correlation matrix across the four datasets. The thirteen subdivisions showed consistent correlation patterns across the four datasets. Similar modularity organization was also achieved between language groups (as shown in Fig. S5).

Figure 8. Conjunction analysis of functional connectivity maps of each module within Broca's region.

Common connections for each of the five modules within Broca's region were shown for the two Chinese datasets (green), two German datasets (blue) and across all four datasets (red). For each pair of figures, the first column shows the anatomical location of each module on the lateral surface view, and the second column shows the conjunction analysis of its functional connectivity patterns across the four datasets (FDR p=0.01, cluster size >50 voxels with 3mm isotropic resolution). Each module showed a distinct functional connectivity profile, but still presented high consistency between language groups.

Tables

Table 1. Detailed information of the subjects from the four rs-fMRI datasets.

The two Chinese datasets were acquired from the Chinese Han and Bai ethnic populations, who speak different Chinese dialects, and the two German datasets were obtained from two local German groups, who are native speakers of German.

Datasets	Populations	Subjects	Age range	Gender	Scanner	Scanning parameters
Dataset 1	Chinese Bai	29	20-36; mean 25.0	16 males	3.0 T Philips	TR=2.0 s, TE=30 ms; Resolution: 3.4×3.4×4.6 mm^3
Dataset 2	Chinese Han	29	22-34; mean 26.0	14 males	3.0 T Philips	TR=2.0 s, TE=30 ms; Resolution: 3.4×3.4×4.6 mm^3
Dataset 3	German	32	22-39; mean 29.0	14 males	3.0 T Siemens	TR=2.2 s, TE=30 ms; Resolution: 3.1×3.1×3.1 mm^3
Dataset 4	German	32	20-31; mean 25.0	13 males	3.0 T Siemens	TR=2.3 s, TE=30 ms; Resolution: 3.0×3.0×4 mm^3

Table 2. Brain regions showing significant difference in connectivity patterns between Chinese and German subjects.

Only two subdivisions and one module showed significant differences in functional connectivity patterns, among which only positive values (i.e. Chinese > German) survived after multiple comparison correction by FDR correction p-value =0.01, cluster size >50 voxels with 3mm isotropic resolution.

Subdivisions /Modules	Brain regions (*Chinese > German*)	Cluster Size	Peaks		MNI coordinates		
			t-score	*z-score*	*x*	*y*	*z*
Cluster 6v2	Left Precentral and Postcentral Gyrus	235	7.84	6.46	-27	-12	72
	Right Inferior Temporal Gyrus	276	6.58	5.68	48	-21	-27
Cluster 45p	Left Middle Frontal Gyrus	117	6.47	5.60	-39	51	24
Module 6v	Left Precentral Gyrus	138	6.95	5.92	-27	-12	72
	Right Inferior Temporal Gyrus	156	6.19	5.41	54	-42	-27